Ratiometric, Fluorescent BODIPY Dye with Aza Crown Ether Functionality: Synthesis, Solvatochromism, and Metal Ion Complex Formation

Wenwu Qin[†], Mukulesh Baruah[†], Michel Sliwa[†], Mark Van der Auweraer[†], Wim M. De Borggraeve[†], David Beljonne[‡], Bernard Van Averbeke[‡], and Noël Boens*[,†]

Department of Chemistry and Institute for Nanoscale Physics and Chemistry (INPAC), Katholieke Universiteit Leuven, Celestijnenlaan 200f-bus 02404, 3001 Leuven, Belgium, Laboratory for Chemistry of Novel Materials, University of Mons-Hainaut, Place du Parc 20, 7000 Mons, Belgium

Received: January 11, 2008

A new pH and metal ion-responsive BODIPY-based fluorescent probe with an aza crown ether subunit has been synthesized via condensation of 4-(1,4,7,10-tetraoxa-13-aza-cyclopentadec-13-yl)-benzaldehyde with the appropriate 1,3,5,7-tetramethyl substituted boron dipyrromethene moiety. Steady-state and time-resolved fluorometries have been used to study the spectroscopic and photophysical characteristics of this probe in various solvents. The fluorescence properties of the dye are strongly solvent dependent: increasing the solvent polarity leads to lower fluorescence quantum yields and lifetimes, and the wavelength of maximum fluorescence emission shifts to the red. The Catalán solvent scales are found to be the most suitable for describing the solvatochromic shifts of the fluorescence emission. Fluorescence decay profiles of the dye can be described by a single-exponential fit in nonprotic solvents, whereas two decay times are found in alcohols. Protonation as well as complex formation with several metal ions are investigated in acetonitrile as solvent via fluorometric titrations. The aza crown ether dye undergoes a reversible (de)protonation reaction ($pK_a = 0.09$) and shows a ~50 nm blue shift in the excitation spectra and a 10-fold fluorescence increase upon protonation. The compound also forms 1:1 complexes with several metal ions (Li^+, Na^+, Mg^{2+}, Ca^{2+}, Ba^{2+}, Zn^{2+}), producing large blue shifts in the excitation spectra and significant cation-induced fluorescence amplifications.

1. Introduction

Fluorescent chemosensors for the measurement of concentrations of analytically and biologically important ions are indispensable tools in numerous fields of modern medicine and science.[1–3] The design and development of fluorescent probes for metal ion analysis remains an active research field.

In recent years, much attention has been focused on the synthesis of 4,4-difluoro-4-bora-3*a*,4*a*-diaza-*s*-indacene[4–6] (boron dipyrromethene or BODIPY) based fluorescent probes and their application as selective and sensitive chemosensors. The abundant applications of boron dipyrromethene derivatives are facilitated by the commercial availability of a range of BODIPY dyes and are illustrated by a selection of recent papers describing BODIPY analogues as fluorescent probes for H^+,[7,8] Na^+,[9] K^+,[10,11] Ca^{2+},[12] Ag^+,[13] Zn^{2+},[14] as photocleavable fluorescent nucleotides in four-color DNA sequencing,[15] and as activity-based fluorescent probes for protein and kinases.[16] BODIPY is a well-known fluorophore characterized by valuable properties such as a high stability toward chemicals and light, relatively high fluorescence quantum yields (often approaching 1.0) and large molar absorption coefficients ($\epsilon > 50000\ M^{-1}\ cm^{-1}$).[7,17–19] Moreover, boron dipyrromethene dyes are excitable with visible light, have narrow emission bandwidths with high peak intensities, and are open to structural modification.

Fluorescent supramolecular systems designed to recognize metal ions typically combine two subunits: a receptor (binding) subunit that selectively binds the target cation and a fluorophore reporter subunit that signals the occurrence of the recognition. To develop a fluorescent ratiometric probe for cations, one generally makes use of an intramolecular charge transfer (ICT) process as the basis for probe design. An intrinsic fluoro ionophore containing an electron-donating group (here an amino group) conjugated to an electron-withdrawing group (here BODIPY) undergoes ICT from the donor to the acceptor upon photoexcitation. The interaction of the cation with the electron-rich donor alters the charge transfer (CT) character of the excited state, and that affects the absorption and/or fluorescence spectral wavelength as well as the fluorescent quantum yield of the fluorophore with a polar excited state, thus producing generally a cation-induced blue shift.

Crown ether derivatives incorporating a fluorescent moiety are attractive tools for optical sensing of metal ions. Crown ethers are well-known to bind alkali-metal and alkaline-earth-metal ions, as well as other cations. Generally, the binding is not selective for a specific ion, but various cations can be complexed by the macrocycle, and the ground-state dissociation constant K_d of the metal ion−crown ether complex depends on factors such as the diameter of the ions relative to the size of the cavity formed by the macrocycle, the number of binding sites on the crown, the type of donor atoms (e.g., oxygen, nitrogen, or sulfur), and the solvent. During the past decade, numerous fluoro ionophores have been built according to this pattern. When the receptor is an aza crown group, the nitrogen atom plays the role of electron donor for both the ICT process and the cation complexation.[20,21]

In the past, the research group of Rurack and Daub has investigated the photophysical behavior of a boron dipyrromethene dye coupled at the *meso* position via a phenyl linker to an aza crown ether that forms 1:1 complexes with various

* To whom correspondence should be addressed. E-mail: Noel.Boens@chem.kuleuven.be. Fax: +32-16-327990.
† Katholieke Universiteit Leuven.
‡ University of Mons-Hainaut.

10.1021/jp800261v CCC: $40.75
Published on Web 06/12/2008

SCHEME 1: Synthesis of 1[a]

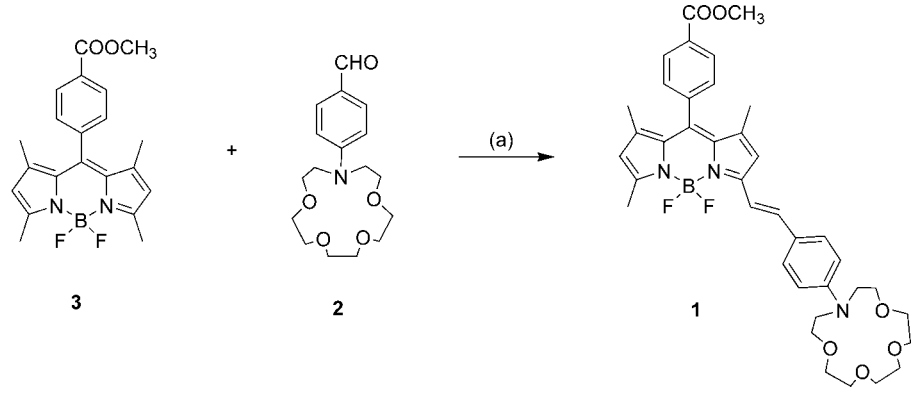

[a] (a) Piperidine, AcOH, toluene, molecular sieves, reflux, 20 h.

alkali and alkaline-earth-metal ions.[18] In these complexes, coordination of the cation to the nitrogen donor atom of the aza crown inhibits the CT process, leading to a huge cation-induced fluorescence enhancement with no cocomittant spectral shift. Only a small bathochromic shift (a few nanometers) in absorption is found. The fluorescence−excitation spectra measured at different emission wavelengths always match and resemble the corresponding absorption spectra. A tetrathia aza crown receptor linked at the *meso* position to a boron dipyrromethene fluorophore via a phenyl group was synthesized by the same group and showed a strong fluorescence enhancement selectively with Hg^{2+}, Ag^{+}, and Cu^{2+} in acetonitrile.[22] Furthermore, a dithia−aza−oxa macrocylce was incorporated via a phenyl linker into a *meso*-substituted BODIPY, yielding amplified fluorescence upon binding of Fe^{3+} ions without pronounced spectral shifts.[23] Recently, we described a fluorescent, *ratiometric* BODIPY-linked aza crown ether chemosensor with high selectivity for K^{+} over other alkali-metal ions that can be excited in the visible wavelength region.[11]

In this work, we synthesized the fluorescent chemosensor **1** with 4,4-difluoro-4-bora-3*a*,4*a*-diaza-*s*-indacene as fluorophore coupled at the 3-position to an aza−tetraoxa macrocycle via an ethenylphenyl linker. The solvent-dependent photophysical characteristics of probe **1** were investigated by steady-state absorption and emission spectroscopy as well as time-resolved fluorometry. From these experiments, we determined the position of the spectral maxima (λ_{abs}, λ_{ex}, and λ_{em}), the full width at half-maximum of the absorption band ($fwhm_{abs}$), the Stokes shifts ($\Delta\bar{\nu} = \bar{\nu}_{abs} - \bar{\nu}_{em}$), the fluorescence quantum yields (ϕ_f) and lifetimes (τ), and the rate constants of radiative (k_f) and nonradiative (k_{nr}) deactivation of compound **1**. We used the Lippert solvent parameter Δf, the normalized $E_T^N(30)$ polarity scale, and the multiparameter Kamlet−Taft and Catalán solvent scales to describe the solvent effect on the fluorescence emission maxima and Stokes shift of **1**. Furthermore, protonation and complex formation of **1** with various metal (Li^{+}, Na^{+}, Ca^{2+}, Mg^{2+}, Ba^{2+}, Zn^{2+}) ions was spectroscopically studied and discussed. Quantum-chemical calculations of the electronic structure and optical properties of **1** were also performed to grasp insight into the origin for the observed spectroscopic changes upon complexation. Finally, the measured ground-state dissociation constants K_d for the formed complexes, the absorption (or excitation) and emission spectral wavelengths in the absence and presence of ions, the fluorescence quantum yields of the free and bound species of **1** are presented and discussed in this study.

2. Results and Discussion

2.1. Synthesis. Fluorescent chemosensor **1** was synthesized by condensation of compounds **2** and **3** using acetic acid—piperidine as a catalyst (Scheme 1).

2.2. Spectroscopic Properties. UV/vis absorption and fluorescence emission spectra of **1** dissolved in a series of solvents of varying polarity are depicted in Figure 1. The photophysical properties of **1** are compiled in Table 1. The main absorption band of **1**, attributed to the 0−0 vibrational band of a strong S_0-S_1 transition, is centered between 608 and 620 nm in the pure solvents (**1**−**18**), in accordance with the results of a related *p*-aminostyryl-linked BODIPY derivative.[24] A shoulder at the short wavelength side can be observed, centered at approximately 575 nm, which is assigned to the 0−1 vibrational band of the same transition. In more polar solvents no vibrational fine structure can be observed. Additionally, weaker absorption bands are found at approximately 450 and 400 nm in all pure solvents, the position of which is not appreciably affected by solvent polarity. These broader and weaker absorption bands are assigned to the S_0-S_2 and S_0-S_3 transitions. The position of the S_0-S_1 absorption band shows minor solvent-dependent shifts, which parallel the polarizability of the solvent,[19] indicating the absence of a ground-state dipole moment (cfr infra). The broadening of the absorption spectra in the more polar solvents, however, suggests a weak charge transfer character for the lowest electronic excitation in the ground-state geometry (vide infra). The typical, narrow BODIPY-like main absorption band[7,17–19] of **1** is only seen in cyclohexane. Indeed, the full width at half-maximum ($fwhm_{abs}$) of the absorption band increases from 997 cm^{-1} in cyclohexane to 1882 cm^{-1} in butanenitrile. The fluorescence−excitation spectra match the absorption spectra in all solvents studied.

Conversely, the fluorescence emission of **1** is strongly solvent dependent. The probe shows a structured emission in the nonpolar solvent cyclohexane, whereas in all other solvents of moderate and high polarity a broad and structureless emission is seen. There is a significant red shift of the emission maximum of approximately 100 nm between cyclohexane and DMSO, indicative of the charge transfer nature of the emitting state. This red shift is accompanied by a loss of fine structure and an increase of the emission bandwidth. Only the emission spectrum in cyclohexane displays the typical BODIPY features,[7,17–19] i.e., a narrow, slightly Stokes-shifted band of mirror image shape.

Inspection of the chemical structure of **1** suggests that the presence of a polar excited state may be responsible for its high solvent sensitivity: the tertiary amino group is electron donating

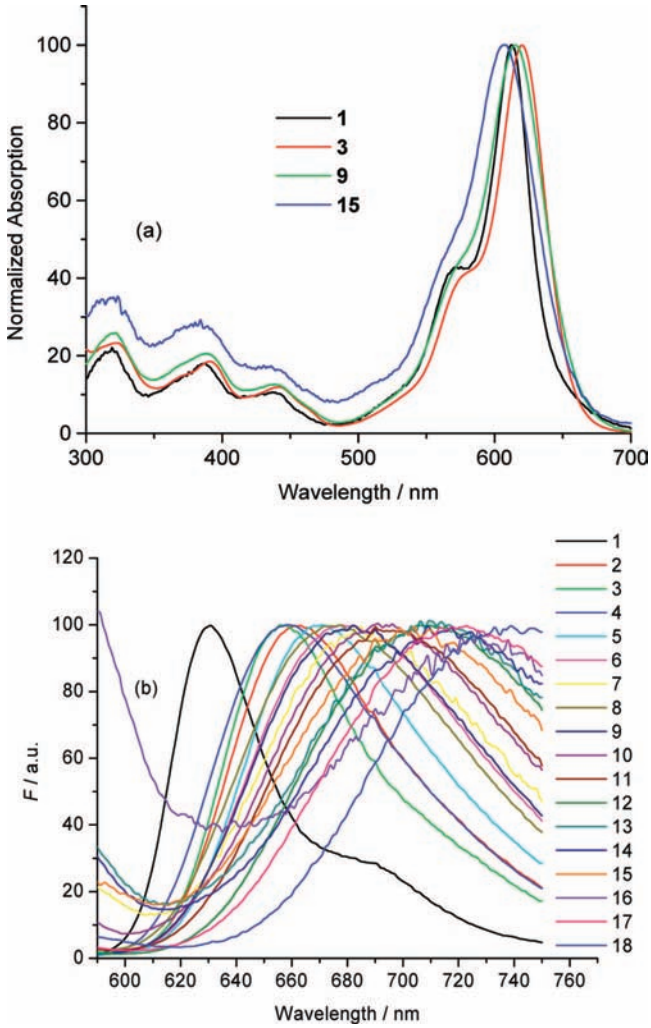

Figure 1. Normalized absorption (a) and emission spectra (b) of **1** (at $\lambda_{ex} = 560$ nm) in several solvents. The numbers refer to the solvents of Table 1: **1** = cyclohexane, **2** = 1,4-dioxane, **3** = toluene, **4** = diethyl ether, **5** = chloroform, **6** = ethyl acetate, **7** = tetrahydrofuran (THF), **8** = 1-decanol, **9** = 1-octanol, **10** = 1-butanol, **11** = 1-propanol, **12** = acetone, **13** = butanenitrile (butyronitrile), **14** = propanenitrile (propionitrile), **15** = methanol, **16** = *N*,*N*-dimethylformamide (DMF), **17** = acetonitrile, **18** = dimethyl sulfoxide (DMSO). Because the absorption spectra all have similar shapes and to keep Figure 1a transparent, only a limited number of absorption spectra are shown.

and the boradiazaindacene subunit is electron-deficient, allowing for the occurrence of a lowest excited state with some CT character.

Next, fluorescence decay traces of **1** in different solvents were collected as a function of emission wavelength. The results of the time-resolved fluorescence experiments are also listed in Table 1. In agreement with the results of two analogous boron dipyrromethene derivatives,[18,24] the time-resolved fluorescence displayed single-exponential decay kinetics in all pure nonprotic solvents studied, with lifetimes ranging from 3.54 ns in cyclohexane to 1.02 ns in DMF. In addition, in the protic solvents (1-decanol, 1-octanol, and 1-butanol), a second, faster subnanosecond component of 666, 417 and 123 ps, respectively, was found. The time-resolved fluorescence profiles of **1** in 1-decanol and 1-octanol were measured at 660, 670, 680, and 700 nm. In 1-butanol, four emission wavelengths were used (670, 680, 690, and 700 nm). The collected fluorescence decay surfaces were analyzed globally as biexponentials with linked decay times τ_1 (slow) and τ_2 (fast). The relative pre-exponential factor α_2 associated with the fast decay component (τ_2) decreased with increasing detection wavelength λ_{em} and became negative at the longest λ_{em} [in 1-decanol $\alpha_2/\alpha_1 = 0.69$ (660 nm), 0.23 (670 nm), 0.01 (680 nm), and −0.25 (700 nm); in 1-octanol $\alpha_2/\alpha_1 = 0.93$ (660 nm), 0.40 (670 nm), 0.13 (680 nm), and −0.20 (700 nm); in 1-butanol $\alpha_2/\alpha_1 = 0.86$ (670 nm), 0.45 (680 nm), 0.22 (690 nm), and −0.03 (700 nm)].

In a previous paper, we studied the influence of methanol and 1-butanol on the solvation dynamics for a similar BODIPY derivative.[24] The fast lifetime component was observed in methanol ($\tau_2 = 14$ ps), but not in aprotic polar solvents as THF, acetonitrile, butanenitrile, ethyl acetate, or dioxane, which have a similar viscosity. We attributed it to the dynamics of hydrogen bonding of the alcohol to the amino group after electron transfer. This is consistent with the weaker interaction between the hydrogen-donating solvents and the amino nitrogen in the excited state compared to the ground state.

The larger values of τ_2 found for dye **1** in 1-butanol (123 ps), 1-octanol (417 ps), and 1-decanol (666 ps) might be due to the higher viscosity of these solvents.[25] It is unlikely that the difference of τ_2 between the different alcohols is related to a difference in solvent polarity. However, the difference in viscosity (2.95 cP for 1-butanol and 13.5 cP for 1-decanol) can explain why the rearrangement of this hydrogen bond after excitation is slower in 1-butanol.

2.3. Solvatochromic Effects. Solvent-dependent spectral shifts are often interpreted in terms of the Lippert−Mataga equation (eq 1), which describes the solvatochromic shifts $\Delta\bar{\nu}$ (expressed in wavenumbers) as a function of the change of the dipole moment $\Delta\mu_{ge} = \mu_e - \mu_g$ of **1** upon excitation. The validity of eq 1 can be checked by using various solvents with different dielectric constants (ϵ) and refractive indices (n) and by plotting $\Delta\bar{\nu}$ as a function of Δf.[26,27]

$$\Delta\bar{\nu} = \frac{2\Delta f}{4\pi\varepsilon_0 hca^3}(\mu_e - \mu_g)^2 + \text{constant} \qquad (1a)$$

$$f(\varepsilon) = \frac{\varepsilon - 1}{2\varepsilon + 1} \quad \text{and} \quad f(n^2) = \frac{n^2 - 1}{2n^2 + 1} \qquad (1b)$$

In eq 1, $\Delta\bar{\nu} = \bar{\nu}_{abs} - \bar{\nu}_{em}$ is the solvatochromic shift (in cm^{-1}) between absorption ($\bar{\nu}_{abs}$) and fluorescence emission ($\bar{\nu}_{em}$) maxima, $\Delta f = f(\epsilon) - f(n^2)$, h is Planck's constant, c is the velocity of light, ϵ_0 is the permittivity of a vacuum, and a is the radius of the cavity in which the solute resides. μ_g and μ_e denote the dipole moments of **1** in ground and excited states, respectively.

The use of eq 1 is limited to transitions where the excited state reached after excitation is also the emissive state (hence for $S_0 \rightarrow S_1$ excitation and equal dipole moments for the Franck−Condon and relaxed excited states) and where the excited-state dipole moment is independent of solvent polarity. Figure 2 represents the Lippert−Mataga plot for **1** in solvents **1**−**18**. The linear relationship of the Stokes shift $\Delta\bar{\nu}$ versus Δf ($0 < \Delta f < 0.31$) is adequate (correlation coefficient $r = 0.920$). For the more polar solvents a small upward deviation from linearity is observed. However, this deviation is less pronounced than for the (dimethylamino)styrylBODIPY.[24]

Contrary to the Lippert solvent parameter Δf, other solvent polarity scales, e.g., the normalized $E_T^N(30)$ scale,[28] take into account the hydrogen-bond-donating and -accepting character of the solvent. Figure 3 shows the Stokes shift $\Delta\bar{\nu}$ for **1** as a function of the $E_T^N(30)$ solvent parameter. It is clear that two different groups of solvents can be distinguished: protic and aprotic. There is an adequate linear relationship between the

TABLE 1: Photophysical Properties of 1 in Several Solvents[a]

	solvent	λ_{abs} (max/nm)	λ_{em} (max/nm)	λ_{ex} (max/nm)	$\Delta\bar{\nu}$ (cm^{-1})	$fwhm_{abs}$ (cm^{-1})	ϕ_f	τ_1 (ns)	τ_2 (ps)	k_f (10^8 s^{1-})	k_{nr} (10^8 s^{1-})
1	cyclohexane	612	631	612	492	997	0.68	3.54		1.92	0.90
2	1,4-dioxane	616	661	616	1105	1308	0.61	3.34		1.83	1.17
3	toluene	620	656	620	885	1182	0.72	3.44		2.09	0.81
4	diethyl ether	608	659	608	1273	1343	0.60	3.49		1.72	1.15
5	$CHCl_3$	615	671	615	1357	1445	0.62	3.45		1.80	1.10
6	$CH_3CO_2CH_2CH_3$	609	678	611	1671	1498	0.50	2.91		1.72	1.72
7	THF	613	685	613	1715	1700	0.50	2.71		1.84	1.84
8	1-decanol	615	677	614	1489	1469	0.43	2.73	666		
9	1-octanol	615	682	614	1597	1528	0.32	2.52	417		
10	1-butanol	612	690	611	1847	1622	0.24	2.02	123		
11	1-propanol	611	690	612	1874	1717	0.17				
12	acetone	610	709	612	2289	1717	0.14				
13	butanenitrile	612	715	612	2354	1882	0.21	1.85		1.14	4.38
14	propanenitrile	610	716	610	2427	1864	0.16	1.55		1.03	5.43
15	CH_3OH	606	704	606	2297	1827	0.08				
16	DMF	619	727	619	2400	1880	0.12	1.02		1.18	8.64
17	CH_3CN	608	723	606	2616	1729	0.08				
18	DMSO	623	739	623	2520	1664	0.068				
19	$CH_3CN + H^+$	556	568	557	380	816	0.75	4.08		1.84	0.61
20	$CH_3OH + H^+$	557	566	557	285	748	0.94	4.03		2.33	0.15

[a] For the time-resolved fluorescence measurements, the samples in solvents **1**−**10**, **13**, **14**, and **16** were excited at 580 nm whereas 543 nm excitation was used for solvents **19** and **20**. For the steady-state and time-resolved fluorescence measurements in solvents **19** and **20**, $HClO_4$ was used as the proton source. The standard errors on τ_1 are ≤10 and ≤15 ps on τ_2. ϕ_f values were determined by excitation at 550 nm (**1**−**18**) and 530 nm (**19**, **20**). The solvents are numbered according to increasing dielectric constant ϵ.

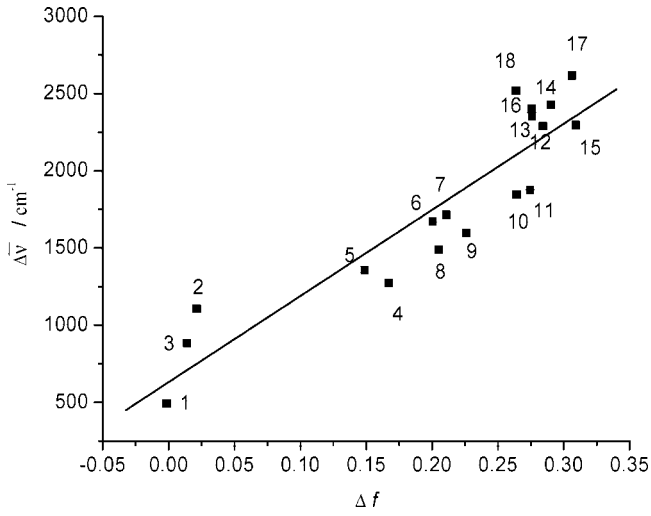

Figure 2. Plot of the Stokes shifts $\Delta\bar{\nu}$ (in cm^{-1}) of **1** in solvents **1**−**18** vs the Lippert solvent parameter $\Delta f = f(\epsilon) - f(n^2)$. The numbers refer to the same solvents as in Figure 1 and Table 1. The straight line is the best fit ($r = 0.920$, slope 5578 cm^{-1}) to the data.

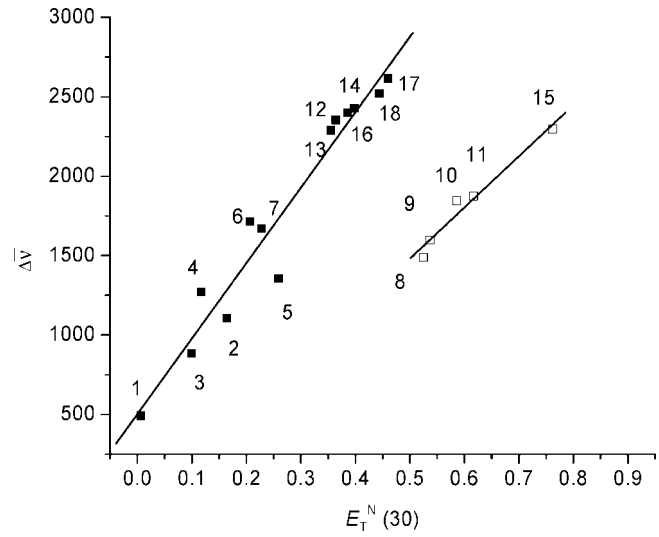

Figure 3. Stokes shift $\Delta\bar{\nu}$ (in cm^{-1}) of **1** as a function of the solvent polarity parameter $E_T^N(30)$. The numbers refer to the same solvents as in Figure 1 and Table 1. The straight line is the best fit ($r = 0.972$) for the nonprotic (filled squares) and ($r = 0.982$) alcohol (open squares) solvents.

Stokes shift and the $E_T^N(30)$ polarity scale for the aprotic ($r = 0.972$) and protic (i.e., alcohol) solvents ($r = 0.982$). A similar linear relationship was found between the fluorescence emission maximum $\bar{\nu}_{em}$ and $E_T^N(30)$ for the aprotic ($r = 0.974$) and protic ($r = 0.969$) solvents (figure not shown). For the alcohol solvents methanol, 1-butanol, 1-propanol, 1-octanol and 1-decanol, the Stokes shift is much smaller than expected on the basis of the $E_T^N(30)$ scale. This parallels the observations made for (dimethylamino)styrylBODIPY.[24]

The solvent effect on $\bar{\nu}_{abs}$, $\bar{\nu}_{em}$, and $\Delta\bar{\nu}$ can also be described on the basis of a multilinear expression (eq 2a):

$$y = y_0 + aA + bB + cC \qquad (2a)$$

in which y_0 stands for the physicochemical property of interest in the absence of solvent (i.e., in the gas phase); a, b, and c are adjustable coefficients that reflect the dependency of the physicochemical property (y) in a given solvent on the various (A, B, C) solvent parameters. At least two different sets of solvent scales can be found in the literature to characterize these solvent properties. In the present analysis, the polarity/polarizability, the acidity, and the basicity of the solvent are considered. Kamlet and Taft[29] put forward the π^*, α, and β parameters to characterize, respectively, the polarity/polarizability, the acidity, and the basicity of a solvent (eq 2b). Conversely, Catalán et al. proposed empirical solvent scales for polarity/polarizability (SPP[30,31]), acidity (SA[31]), and basicity (SB[31,32]) to describe the respective properties of a given solvent (eq 2c).

$$y = y_0 + a_\alpha\alpha + b_\beta\beta + c_{\pi^*}\pi^* \qquad \text{(Kamlet − Taft)} \quad (2b)$$

$$y = y_0 + a_{SA}SA + b_{SB}SB + c_{SPP}SPP \qquad \text{(Catalán)} \quad (2c)$$

Table 2 compiles the estimated coefficients y_0, a, b, c (see eq 2) and correlation coefficients (r) for the multiple linear

TABLE 2: Estimated Coefficients (y_0, a, b, c; Eq 2), Their Standard Errors, and Correlation Coefficients (r) for the (Multiple) Linear Regression Analysis of the Absorption ($\bar{\nu}_{abs}$) and Fluorescence Emission Maxima ($\bar{\nu}_{em}$), and the Stokes Shifts $\Delta\bar{\nu}$ of 1 in Solvents 1−18 (Table 1) as a Function of the Kamlet−Taft (Eq 2b: Acidity α, Basicity β, and Polarity/Polarizability π^*) and Catalán (Eq 2c: Acidity SA, Basicity SB, and Polarity/Polarizability SPP) Solvent Scales

Kamlet−Taft	y_0 (cm^{-1})	a_α	b_β	c_{π^*}	r
$\bar{\nu}_{abs}$	$(16.4 \pm 0.1) \times 10^3$	$(1 \pm 1) \times 10^2$	$(-1 \pm 2) \times 10^2$	$(-1 \pm 2) \times 10^2$	0.381
$\bar{\nu}_{em}$	$(16.1 \pm 0.2) \times 10^3$	$(-1 \pm 2) \times 10^2$	$(-5 \pm 3) \times 10^2$	$(-2.2 \pm 0.3) \times 10^3$	0.932
$\bar{\nu}_{em}$	$(15.9 \pm 0.2) \times 10^3$			$(-2.4 \pm 0.3) \times 10^3$	0.893
$\Delta\bar{\nu}$	$(2 \pm 2) \times 10^2$	$(2 \pm 3) \times 10^2$	$(4 \pm 4) \times 10^2$	$(2.2 \pm 0.4) \times 10^3$	0.874
Catalán	y_0 (cm^{-1})	a_{SA}	b_{SB}	c_{SPP}	r
$\bar{\nu}_{abs}$	$(16.0 \pm 0.2) \times 10^3$	$(3 \pm 2) \times 10^2$	$(-1 \pm 1) \times 10^2$	$(-1 \pm 3) \times 10^2$	0.797
$\bar{\nu}_{em}$	$(19.0 \pm 0.3) \times 10^3$	$(-1 \pm 2) \times 10^2$	$(2 \pm 2) \times 10^2$	$(-5.5 \pm 0.3) \times 10^3$	0.978
$\bar{\nu}_{em}$	$(19.0 \pm 0.2) \times 10^3$			$(-5.4 \pm 0.3) \times 10^3$	0.977
$\Delta\bar{\nu}$	$(-2.5 \pm 0.4) \times 10^3$	$(3 \pm 3) \times 10^2$	$(-3 \pm 2) \times 10^2$	$(5.5 \pm 0.5) \times 10^3$	0.957

regression analysis of the absorption ($\bar{\nu}_{abs}$) and fluorescence emission maxima ($\bar{\nu}_{em}$), and the Stokes shift $\Delta\bar{\nu}$ of **1** as a function of the Kamlet−Taft (eq 2b) and Catalán (eq 2c) solvent scales for the pure solvents (**1**−**18** of Table 1). The Kamlet−Taft solvatochromic parameters α, β, and π^* parameters are taken from ref 33, whereas the Catalán solvent parameters SA, SB, and SPP are from refs 30–32. Both sets of solvent scales produce similar qualitative results, although the Catalán scales yield consistently better fits for $\bar{\nu}_{abs}$, $\bar{\nu}_{em}$, and $\Delta\bar{\nu}$ (as judged by the correlation coefficient r as quality-of-fit criterion).

For both sets of solvent scales, the estimated coefficients describing the solvent polarity/polarizability (large and negative c_{SPP} and c_{π^*} values) indicate that the solvent polarity/polarizability is the main parameter responsible for the shift of the fluorescence emission band ($\bar{\nu}_{em}$). Fitting a linear equation with the solvent scale SPP as the only independent variable to $\bar{\nu}_{em}$ (eq 2c with $a_{SA} = 0$ and $b_{SB} = 0$) confirms that the polarity/polarizability of the solvent is the most important factor determining the position of the fluorescence emission maximum $\bar{\nu}_{em}$. Indeed, this linear fit (Catalán, Table 2) has an almost identical r value (0.977) as the multilinear fit ($r = 0.978$). A comparable result is obtained for the Kamlet−Taft scale: if the solvent parameter π^* is used as the only independent variable in the linear equation to fit $\bar{\nu}_{em}$ (eq 2b with $a_\alpha = 0$ and $b_\beta = 0$), the obtained correlation coefficient ($r = 0.893$) is fractionally smaller than for the multilinear fit ($r = 0.932$).

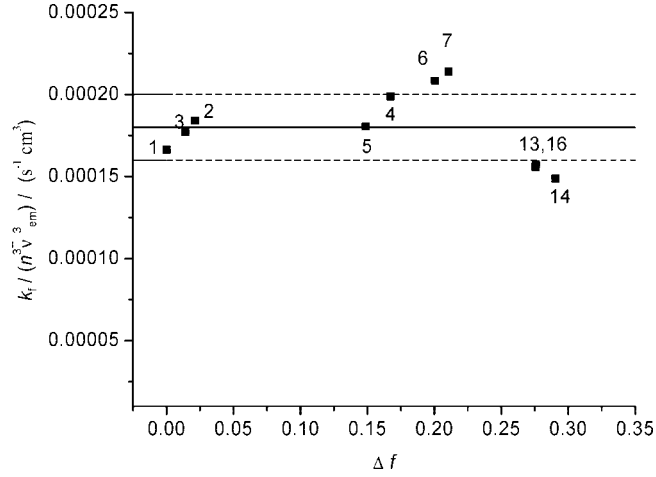

Figure 4. Plot of $k_f/(n^3\,\bar{\nu}_{em}{}^3)$ vs Δf for **1**. The numbers refer to the same solvents as in Figure 1 and Table 1. The solid line indicates the average value; the dashed lines represent ± one sample standard deviation.

The small solvatochromism of **1** for absorption is noteworthy. Indeed, the data of Table 2 indicate that $\bar{\nu}_{abs}$ does not depend on solvent polarity/polarizability, acidity, or basicity. However, this small change may reflect just a slight change in polarizability on the environment of the chromophore. Indeed, when one plots $\bar{\nu}_{abs}$ as a function of the Catalán solvent polarizability parameter SP (SP[34] scale) for solvents **1**−**18** of Table 1, an excellent linear relationship (eq 3, $r = -0.952$) is found between $\bar{\nu}_{abs}$ and SP (Figure S1, Supporting Information, SI),

$$\bar{\nu}_{abs} = \bar{\nu}^0_{abs} + a_{SP}SP \tag{3}$$

with $\bar{\nu}^0_{abs} = (17.6 \pm 0.1) \times 10^3$ cm^{-1} and $a_{SP} = (20 \pm 2) \times 10^2$. This clearly indicates that the absorption spectra depend only on the change of polarizability of the environment of the chromophore.

When the fluorescence decays are single-exponential, the rate constants of fluorescence (k_f) and nonradiative deactivation (k_{nr}) can be calculated from the measured fluorescence quantum yield ϕ_f and lifetime τ according to

$$k_f = \phi_f/\tau \tag{4a}$$

$$k_{nr} = (1 - \phi_f)/\tau \tag{4b}$$

The data in Table 1 show that k_f remains almost constant in low-polarity ($\epsilon < 8$) solvents and decreases in high polarity ($\epsilon > 20$) solvents such as butanenitrile, propanenitrile, and DMF. Because k_f is proportional to the product of the squared transition dipole moment $\langle\psi_G\mu\psi_E\rangle^2$, n^3, and $\bar{\nu}_{em}{}^3$,[35]

$$k_f = \frac{64\pi^4}{3h} n^3\,\bar{\nu}_{em}{}^3\langle\psi_G|\hat{\mu}|\psi_E\rangle^2 \tag{5}$$

we plotted $k_f/(n^3\,\bar{\nu}_{em}{}^3)$ of **1** vs Δf (Figure 4) to check the solvent dependence of the transition dipole. In eq 5, $\hat{\mu}$ stands for the dipole moment operator. The ratio $k_f/(n^3\,\bar{\nu}_{em}{}^3)$ remains practically constant [$(1.8 \pm 0.2) \times 10^{-4}$ s^{-1} cm^3) over the whole Δf range ($0 < \Delta f < 0.31$)]. This indicates that the transition dipole moment $\langle\psi_G\mu\psi_E\rangle$ stays nearly constant, even in more polar solvents. In this aspect, compound **1** differs from the (dimethylamino)styrylBODIPY.[24]

Figure 5 shows the plot of log k_{nr} as a function of $\bar{\nu}_{em}$. The increase of k_{nr} upon increasing solvent polarity can be rationalized if k_{nr} can be attributed primarily to internal conversion.[24]

2.4. pH Dependence of the Absorption and Fluorescence Spectra in Acetonitrile Solution. Protonation of the tertiary amine function of **1** drastically alters its electron-donating properties and consequently decreases the polar character of the excited state. In acidified acetonitrile, this produces the typical

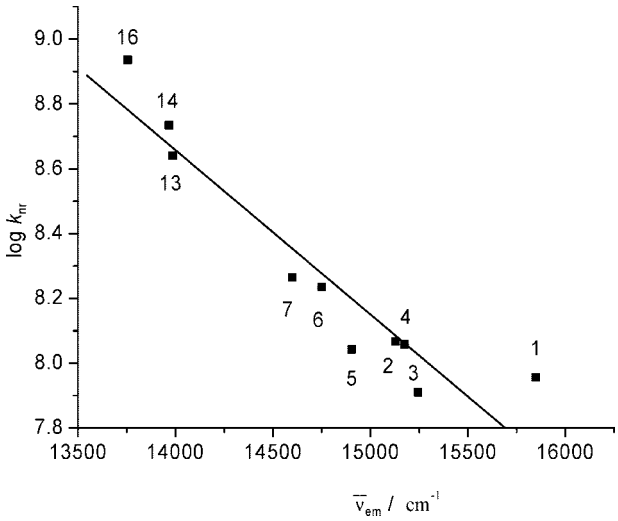

Figure 5. Plot of log k_{nr} vs $\bar{\nu}_{em}$ (in cm^{-1}) for **1**. The numbers refer to the same solvents as in Figure 1 and Table 1. The straight line is the best fit ($r = -0.942$) to the data.

BODIPY-like narrow absorption and emission bands with a very high fluorescence yield[7,17–19] (cfr infra). The pH-dependent effects on the absorption spectra of **1** are displayed in Figure 6a. The absorption spectra of **1** show a decrease of the absorbance band with a maximum at 608 nm with increasing $HClO_4$ concentration (i.e., lower pH) and a simultaneous increase of the absorption at 555 nm. Varying the pH also gives rise to two isosbestic points at 568 and 465 nm. The lowest-energy absorption band of the ammonium form of the dye is blue-shifted by ~50 nm compared to that of the neutral amine form. The width of the absorption band of the neutral amine (fwhm$_{abs}$ = 1729 cm^{-1}) is ~50% smaller in the ammonium form (fwhm$_{abs}$ = 816 cm^{-1}), similar to the values found in apolar solvents for the neutral form.

The fluorescence−excitation (λ_{em} = 660 nm) and emission spectra (λ_{ex} = 530 nm) of **1** in acetonitrile are shown as a function of pH in Figure 6b,c, respectively. In the same way as the absorption spectra, the fluorescence−excitation maximum at 608 nm (neutral amine form) moves to 555 nm (positively charged ammonium form) at lower pH. The highest ϕ_f value (0.80, determined at λ_{ex} = 530 nm) is found for the ammonium form (at the lowest pH, namely −1.13). The apparent pH independence of the spectral shape of the main emission band and the maximum of the fluorescence spectra (Figure 6c) are due to the lower emission quantum yield (Figure S2, Supporting Information) and the small absorption coefficient of the neutral form (compared to the protonated form) at 530 nm.

The acidity constant K_a (=K_d in eq 6 when X = H^+) and the stoichiometry (n) of the binding of H^+ by the amine function of **1** were determined by fitting eq 6 (*direct* fluorometric titration) or eq 7 (*ratiometric* fluorometric titration) to the fluorescence−excitation or emission spectral data F (eq 6) or their ratios R (eq 7), measured as a function of cation concentration [X].

$$F = \frac{F_{max}[X]^n + F_{min}K_d}{K_d + [X]^n} \quad (6)$$

In eq 6, F stands for the fluorescence signal at [X], whereas F_{min} and F_{max} denote the fluorescence signals at minimal and maximal [X], respectively, and n is the number of cations bound per probe molecule.

$$R = \frac{R_{max}[X]^n + R_{min}K_d\xi}{K_d\xi + [X]^n} \quad (7)$$

In the *excitation* ratiometric method, one measures $R = F(\lambda_{em},\lambda^1_{ex})/F(\lambda_{em},\lambda^2_{ex})$ at a common emission wavelength, λ_{em}, and two different excitation wavelengths, λ^1_{ex} and λ^2_{ex}. R_{min} is

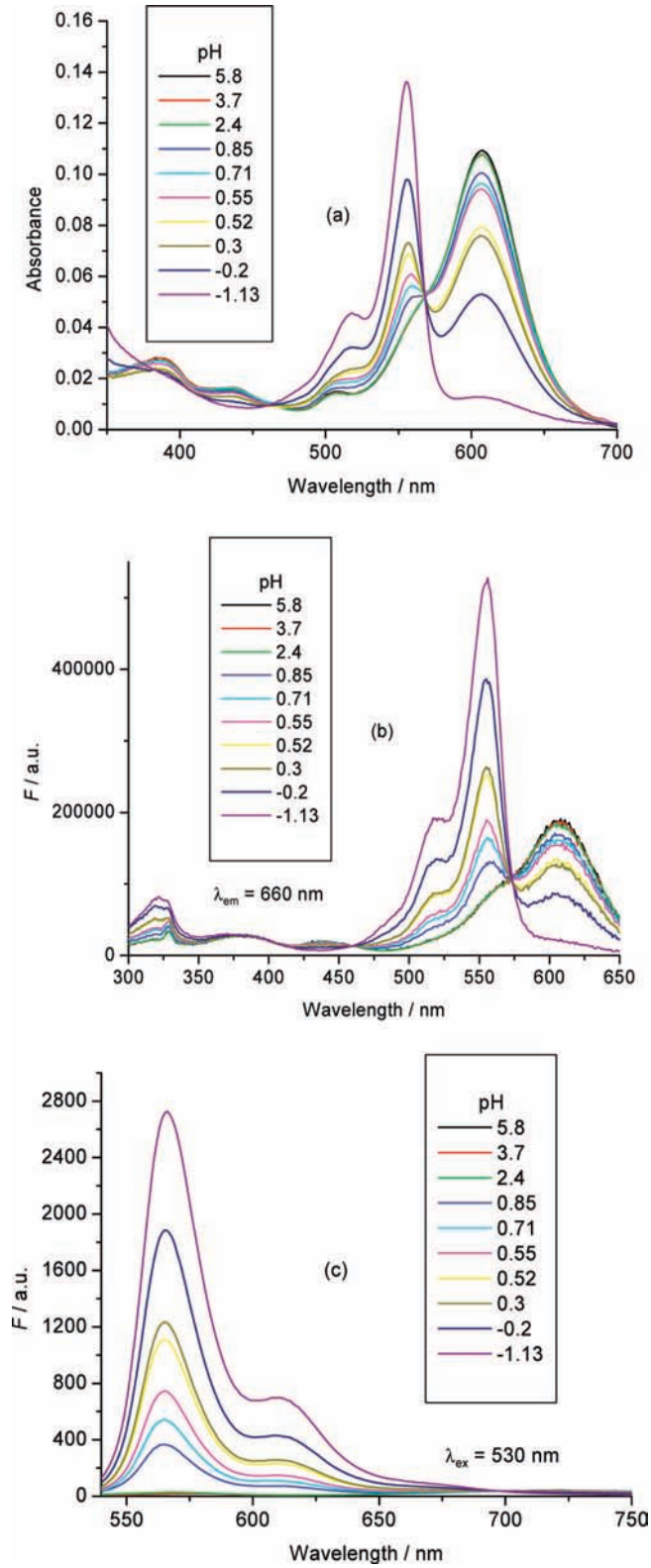

Figure 6. (a) Absorption spectra of **1** in acetonitrile solution as a function of pH. (b) Corresponding fluorescence−excitation spectra (λ_{em} = 660 nm). (c) Corresponding emission spectra (λ_{ex} = 530 nm).

TABLE 3: Spectral Characteristics of 1 in the Absence and Presence of Various Cations in Acetonitrile

complex	λ_{abs} (max/nm)	isobestic points (nm)	λ_{em} (max/nm)	λ_{ex} (max/nm)	$\Delta\bar{\nu}$ (cm^{-1})	K_d (mM)	ϕ_f
1	608		723	608	2616		0.08
1$-H^+$	555	465, 568	565	555	319	850	0.80
1$-Li^+$	594	485, 590	700	589	2549	0.919	0.18
1$-Na^+$	579	413, 475, 585	708	575	3147	4.4	0.16
1$-Mg^{2+}$	562	472, 572	573	562	342	71	0.80
1$-Ca^{2+}$	563	360, 475, 577	569	563	187	10.1	0.24
1$-Ba^{2+}$	556	340, 470, 568	567	556	349	0.45	0.92
1$-Zn^{2+}$	558	473, 568	565	558	222	5	0.59

the ratio of the fluorescence intensities at two distinct excitation wavelengths and one emission wavelength of the free form of the indicator (minimum [X]), R_{max} represents the ratio of the fluorescence intensities of the bound form of the indicator (maximum [X]), R denotes the ratio of the fluorescence intensities corresponding to intermediate [X], and $\xi = F_{min}(\lambda_{em},\lambda^2_{ex})/F_{max}(\lambda_{em},\lambda^2_{ex})$.

In the *emission* ratiometric method one measures $R = F(\lambda^1_{em},\lambda_{ex})/F(\lambda^2_{em},\lambda_{ex})$ at the indicated wavelengths as a function of cation concentration [X]. In this case, ξ is defined as $\xi = F_{min}(\lambda^2_{em},\lambda_{ex})/F_{max}(\lambda^2_{em},\lambda_{ex})$.

The average pK_a value obtained from direct fluorometric titrations (eq 6) using excitation and emission spectra was found to be 0.09 ± 0.05 and gave a well-defined 1:1 stoichiometry between **1** and H^+, indicative of ammonium ion formation. Because large spectral shifts are observed in the fluorescence−excitation spectra, the *ratiometric* method (eq 7) can be used to estimate values of K_a. The ratio $R = F(\lambda_{em},\lambda^1_{ex})/F(\lambda_{em},\lambda^2_{ex})$ of two fluorescence−excitation intensities (at $\lambda^1_{ex} = 555$ nm and $\lambda^2_{ex} = 575$ nm) with observation at $\lambda_{em} = 660$ nm as a function of pH was used to estimate $K_a\xi$, n, R_{min}, and R_{max}. The obtained value for pK_a (0.06) is in good agreement with that measured by the *direct* titration method. The estimated n value indicates that **1** binds one proton.

2.5. Complex Formation between 1 and Various Metal Ions in Acetonitrile Solution. Complex formation was investigated for **1** with alkali (Li^+, Na^+, K^+, Cs^+), alkaline-earth (Mg^{2+}, Ca^{2+}, Ba^{2+}), and transition metal ions (Ni^{2+}, Cu^{2+}, Zn^{2+}, Cd^{2+}) in acetonitrile. The results are summarized in Table 3.

Upon addition of K^+, Cs^+, Ni^{2+}, Cu^{2+}, and Cd^{2+} in the μM concentration range to a mM solution of **1** in acetonitrile, no change in the UV/vis absorption and fluorescence spectra could be found.

Of the alkali-metal ions, only Li^+ (between 0 and 5 mM) and Na^+ (between 0 and 14.2 mM) produced spectral changes of **1**. The lowest-energy absorption band of **1** shifts hypsochromically by ~10 nm, from 608 in Li^+ free environment to 594 nm when Li^+ is added to the CH_3CN solution (Figure S3, SI). The relative contributions of the 608/594 nm signals change with varying [Li^+] and show isosbestic points at 485 and 590 nm. Similar changes were observed in the fluorescence−excitation spectra. The maximum of the fluorescence emission band shifts from 723 nm in ion-free acetonitrile to 700 nm in the presence of Li^+ and is accompanied by a increase in intensity. The low ϕ_f value for free **1** (0.08) can be attributed to the CT character of the excited state. Upon binding Li^+, the electron-donating properties of the amine are reduced, decreasing the CT-character of the excited state and causing a 2-fold amplification of the fluorophore's quantum yield. The average K_d value for the Li^+ complex with **1**, determined by direct fluorometric titration (eq 6) of excitation and emission spectral data F, equals 0.98 ± 0.07 mM. The excitation ratiometric titrations gave $K_d = 0.81$ ± 0.04 mM. The spectral changes observed when Na^+ is added to the acetonitrile solution of **1** are very similar to those for Li^+ (Table 3, Figure S4, SI), but the blue shift upon complex formation is larger. An average K_d value of 4.3 ± 0.3 mM was obtained for the Na^+ complex with **1** by direct fluorometric titration, in excellent agreement with the K_d value obtained from excitation ratiometric measurements (4.4 ± 0.1 mM).

The addition of alkaline-earth metal (Mg^{2+}, Ca^{2+}, Ba^{2+}) perchlorates to a solution of **1** in acetonitrile results in a significant (approximately 50 nm) hypochromic shift of the absorption spectrum. The absorption spectra of **1** in the presence of Mg^{2+} are illustrated in Figure 7. The spectral changes observed for Ca^{2+} (Figure S5, SI) and Ba^{2+} are similar to those depicted in Figure 7 for Mg^{2+}.

The addition of Mg^{2+}, Ca^{2+}, and Ba^{2+} to a solution of **1** in CH_3CN strongly affects the absorption spectra. Upon increasing the metal ion concentration, the lowest energy absorption band (with maximum at 608 nm in the absence of metal ions) decreases in intensity whereas a new peak appears at approximately 560 nm whose intensity increases with higher metal ion concentration. The $fwhm_{abs}$ of the new peak in the presence of Mg^{2+}, Ca^{2+}, and Ba^{2+} is 863, 1014, and 816 cm^{-1}, respectively, much less than in the absence of ions (1729 cm^{-1}). Isosbestic points (Table 3) are observed in the spectra as a function of the metal ion concentration.

The fluorescence emission spectra of **1** as a function of [Mg^{2+}] also are shown in Figure 7. In salt-free CH_3CN, the emission spectrum of **1** displays a weak, broadband with a maximum at ~723 nm, attributed to the formation of a polar excited state with CT character. Upon increasing [Mg^{2+}], the emission originating from the polar excited state remains nearly constant, whereas the emission band with a maximum at 573 nm and a shoulder at 625 nm originating from the nonpolar excited state increases its intensity. The latter emission band in the presence of Mg^{2+} is the mirror image of the absorption (or excitation) band, corresponding to the S_1-S_0 transition (0−0 and 0−1 vibrational progression, respectively) of the complex. There is a 10-fold fluorescence amplification of **1** in the presence of Mg^{2+}. K_d values of the **1**$-Mg^{2+}$ complexes were determined from direct excitation and emission fluorometric titrations and ratiometric excitation fluorometric titrations, yielding a median K_d value of 71 ± 18 mM.

The emission spectral changes of **1** in the presence of Ba^{2+} (Figure S5, SI) are similar to those of Mg^{2+}. The ϕ_f value of **1** in the presence of Ba^{2+} is 0.92. The average K_d value of the **1**$-Ba^{2+}$ complex estimated via direct fluorometric titrations using excitation spectra was found to be 0.45 ± 0.18 mM, indicating that **1** binds Ba^{2+} much better than Mg^{2+}.

Addition of Ca^{2+} to a solution of **1** in CH_3CN enhances the fluorescence intensity of both emission bands originating from the polar and apolar excited states (Figure 7), yielding a ϕ_f value of 0.24. The K_d value of the **1**$-Ca^{2+}$ complex estimated from direct excitation and emission fluorometric titrations ($K_d = 9.7$ ± 1.6

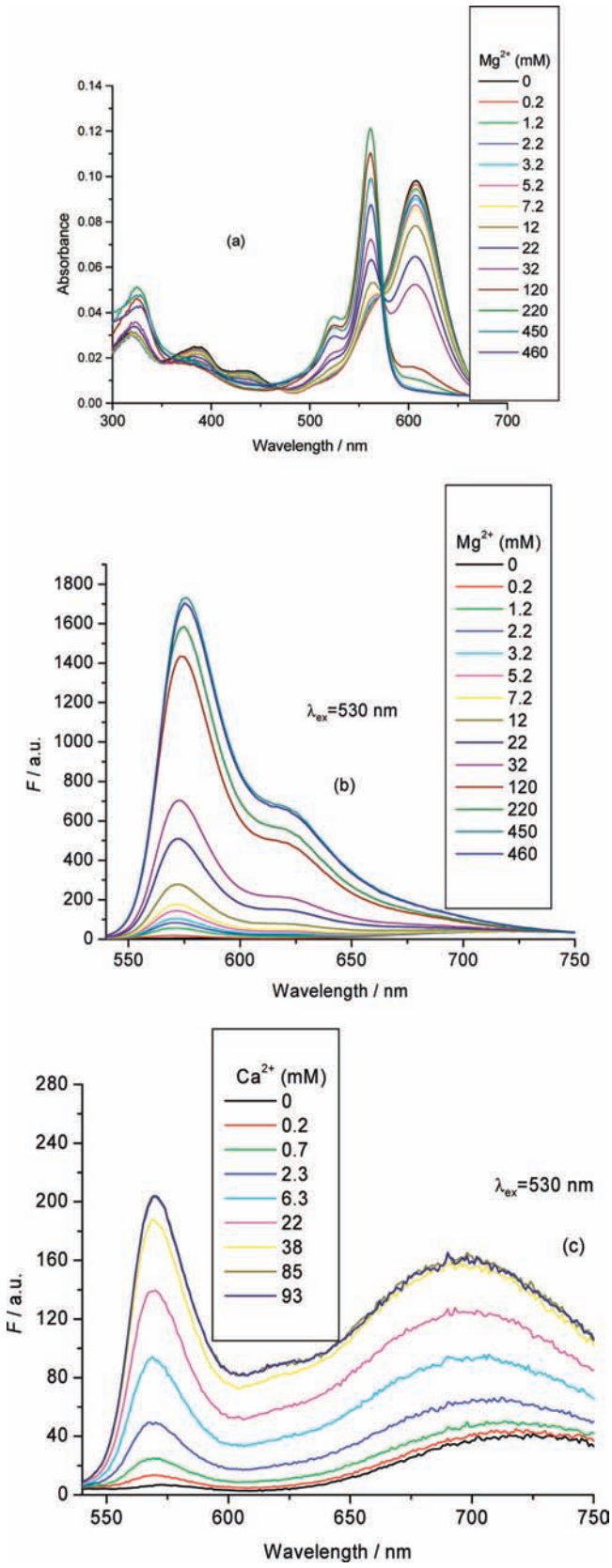

Figure 7. (a) Absorption spectra of **1** in acetonitrile solution as a function of $[Mg^{2+}]$. (b) Corresponding emission spectra ($\lambda_{ex} = 530$ nm). (c) Corresponding emission spectra ($\lambda_{ex} = 530$ nm) of **1** as function of $[Ca^{2+}]$.

mM) is in good agreement with that recovered from ratiometric excitation and emission titrations ($K_d = 10.6 \pm 1.4$ mM).

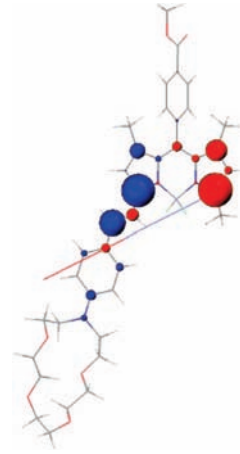

Figure 8. DFT//B3LYP optimized ground-state geometry and INDO/SCI transition density distribution for the lowest optical transition of **1**.

The changes observed in the absorption and emission spectra of the **1**−Zn^{2+} complex (Figure S6, SI) are similar to those found for **1** in the presence of Mg^{2+} and Ba^{2+}. There is a large fluorescence enhancement of **1** in the presence of Zn^{2+} with ϕ_f increasing to 0.59. K_d values of the **1**−Zn^{2+} complexes were determined from direct and ratiometric excitation and emission fluorometric titrations and yielded an average K_d value of 4.9 ± 1.5 mM.

2.6. Quantum-Chemical Calculations. The equilibrium geometries for the pristine, protonated and complexed (with Na^+) forms of **1** were optimized using a combination of force field and density functional theory methods; these were subsequently used as input for INDO/SCI calculations of the spectroscopic properties (see Theoretical Methodology for details). The transition densities (providing a local map of the transition dipole moment), as computed at the INDO/SCI level for excitation from the ground state to the lowest optically allowed excited state of the pristine molecule, are depicted in Figure 8. For the molecule in the gas phase, the lowest optical transition (and the frontier, i.e., HOMO and LUMO, molecular orbitals) is found to be primarily localized on the BODIPY core, yet with sizable contributions on the styryl arm. The change in dipole moment when going from the ground state to the excited state only amounts to 3.7 D in the ground-state geometry (i.e., for a vertical absorption process). As described in detail for a closely related *p*-aminostyryl-linked BODIPY derivative, [24] the CT contributions to the excited-state wave function are largely enhanced upon geometric relaxation in the excited state and in solvents of increasing polarity.

The vertical transition energies calculated for **1**, its protonated form and the Na^+ complex are compared to the corresponding experimental values in Table 4. The measured spectral shifts are well reproduced by the calculations, although the predicted blue shift for the protonated molecule is underestimated compared to the experimental value. The shift in the optical transition energy upon complexation can arise from two interconnected origins: a change in the conformation of the molecule (indirect effect) and/or a change in the electron-donating character of the amino moiety bearing the crown ether in the presence of the cation (direct effect).

To disentangle these effects, we have repeated the INDO/SCI calculations on the geometry of the complex after removing the sodium ion. The results, reported in Table 4, indicate that the largest contribution to the total blue shift stems from the interaction between the nitrogen lone pair and the ion and the resulting

TABLE 4: Spectroscopic Properties Estimated at the INDO/SCI Level on the Basis of DFT/B3LYP/6-311g Geometries**

molecule	E_{abs} theory (eV)	E_{abs} exp (eV)	$E - E(\mathbf{1})$ theory (eV)	$E - E(\mathbf{1})$ exp (eV)	conformational shift[a]	electron density of N in HOMO[b]
1	2.28	2.04	0	0		0.0611
1−H^+	2.38	2.23	0.10	0.19		0.0003
1−Na^+	2.4	2.14	0.12	0.10	0.03	0.0045

[a] Shift calculated on the basis of the optimized structure of **1**-Na^+ but without the ion, see text. [b] Electron density (square of the LCAO coefficient) over the N atom of the aza crown in the HOMO molecular orbital.

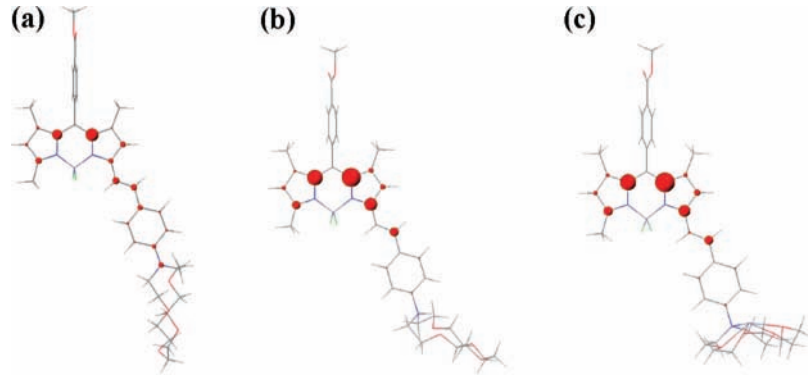

Figure 9. INDO electronic density in the HOMO level of the pristine (a), protonated (b) and Na^+ complexed (c) form of **1**.

decoupling of the π-system. Note that this differs substantially from the conclusions drawn from a previous study on a related fluoro ionophore lacking a styryl unit in between the BODIPY core and the aza crown ether, where the conformational contribution was found to dominate.[11] The effect of complex formation can be better appreciated by considering the electronic density over the HOMO orbitals displayed in Figure 9 (see also Table 4). One can clearly see that the electronic density on the nitrogen atom is strongly reduced in the HOMO level in the presence of the cation. Hence, the lowest optical transition in the complex has a lower charge transfer character than in the pristine molecule, which results in the observed blue shift.

In the protonated form, the hybrization of the nitrogen atom in the aza crown ether moiety changes from sp^2 to sp^3. As for the complexation by alkaline ions, the donating strength of the aza group is strongly reduced upon protonation, as illustrated by the HOMO electron density in Figure 9 and Table 4, and the vertical transition energy is shifted to shorter wavelengths.

3. Conclusion

We have synthesized the visible light excitable, fluorescent BODIPY-based dye **1**, which shows strongly solvent-dependent fluorescence emission properties. Comparison of the solvent-dependent absorption and emission properties of amino-substituted boron dipyrromethene dyes[24] indicates that in nonpolar solvents emission occurs mainly from a nonpolar excited state, whereas in more polar solvents a polar excited state is formed. The fluorescence quantum yield and the lifetime decrease in polar solvents in conjunction with large bathochromic shifts.

Protonation as well as complex formation with metal ions obstruct the formation of the polar excited state and lead to a large increase in the fluorescence of the nonpolar state. The new boradiazaindacene dye is an example of a very sensitive fluorescent probe for several metal ions displaying large absorption and fluorescence changes in an analytically useful wavelength region.

4. Experimental Section

4.1. Materials, NMR and Mass Spectra. All solvents for the spectroscopic measurements were of spectroscopic grade and were used without further purification. Metal perchlorates were of highest purity available and were dried in a vacuum oven before use. The chemicals for the synthesis were of reagent grade quality, procured from commercial sources, and used as received. Boron trifluorode etherate was ca. 48% BF_3. ^1H and ^{13}C NMR spectra were recorded on instruments operating at a frequency of 300 MHz for ^1H and 75 MHz for ^{13}C. ^1H NMR spectra were referenced to tetramethylsilane (0.00 ppm) as an internal standard. Chemical shift multiplicities are reported as s = singlet, d = doublet, and m = multiplet. ^{13}C spectra were referenced to the $CDCl_3$ (77.67 ppm) signal. Mass spectra were recorded in CI and EI mode.

4.2. Synthesis of 2 and 3. Compound **2** was synthesized by Vilsmeier formylation of commercially available phenyl-aza-15-crown-5-ether.

^1H NMR (300 MHz, $CDCl_3$): δ 9.8 (s, 1H), 7.7 (d, 2H, J = 9.14 Hz), 6.7 (d, 2H, J = 9.14 Hz), 3.6−3.9 (m, 20H). MS: (CI) 324 (M+1, 100%).

Compound **3** was synthesized following a literature procedure.[8]

4.3. Synthesis of 3-[2-(4-Aza-phenyl-15-crown-5-ether) ethenyl]-4,4-difluoro-8-[4-(methoxycarbonyl)phenyl]-1,5,7-trimethyl-3*a*,4*a*-diaza-4-bora-*s*-indacene, 1. An 80 mg (2.5 mmol) sample of **2** and 76 mg (2 mmol) of **3** were dissolved in 6 mL of dry toluene. Dry piperidine (0.1 mL) and 0.1 mL of acetic acid were added to the mixture. The reaction mixture was heated to reflux with some molecular sieves for 20 h. After cooling to room temperature, the reaction mixture was purified by column chromatography on silica gel using ethylacetate/heptane (1:2 v/v) as eluent. The collected deep blue fraction was recrystallized from chloroform/hexane to yield 38 mg (28% yield) of deep purple powder of compound **1**.

^1H NMR (300 MHz, $CDCl_3$): δ 8.20 (d, 2H, J = 8.2 Hz), 7.51 (d, 1H, J = 15.4 Hz), 7.48 (d, 2H, J = 8.6 Hz), 7.46 (d, 2H, J = 8.2 Hz), 7.25 (d, 1H, J = 16.2 Hz), 6.69 (d, 2H, J = 8.6 Hz), 6.61 (s, 1H), 5.98 (s, 1H), 3.99 (s, 3H), 3.79−3.65 (m, 20H), 2.59, (s, 3H), 1.42 (s, 3H), 1.37 (s, 3H). LRMS (EI, 70 eV) 687 (M^+, 100). HRMS (EI) calc for $C_{38}H_{44}BF_2N_3O_6$ 687.3291, found 687.3278.

4.4. Steady-State UV/Vis and Fluorescence Spectroscopy. UV/vis spectra were recorded on a Perkin-Elmer Lambda 40 UV/vis spectrophotometer, and for the corrected steady-state excitation and emission spectra, a SPEX Fluorolog was employed. For the determination of the fluorescence quantum yields ϕ_f in solvents **1**−**18**, dilute solutions with an absorbance below 0.1 at $\lambda_{ex} = 550$ nm were used. Cresyl violet in methanol ($\phi_f = 0.55$) was used as the fluorescence standard.[36] For solvents **19** and **20**, ϕ_f was determined by excitation at 530 nm. The ϕ_f values reported in Table 1 are the averages of multiple (generally four), fully independent measurements. The ϕ_f values as a function of pH were measured by excitation at 530 nm. In all cases, correction for the refractive index was applied. All spectra were recorded at room temperature on nondegassed samples.

4.5. Time-Resolved Fluorescence Spectroscopy. Fluorescence decay traces of **1** were recorded at several emission wavelengths by the single-photon timing method.[37] Details of the experimental procedures[38] have been described elsewhere. The samples were excited at a repetition rate of 8.18 MHz with 543 or 580 nm light using the frequency-doubled output from an OPO pumped by a picosecond Ti:sapphire laser. Fluorescence decay histograms were collected under magic angle in 4096 channels using 10 × 10 mm cuvettes. The absorbance at the excitation wavelength was always below 0.1. All lifetime measurements were performed on nondegassed samples at 20 °C. Histograms of the instrument response functions (using a LUDOX scatterer) and sample decays were recorded until they typically reached 10^4 counts in the peak channel. The measured width at half-maximum of the instrument response function was ~30 ps.

The fitting parameters were determined by nonlinear least-squares estimation by minimizing the global reduced χ_g^2:

$$\chi_g^2 = \sum_l^q \sum_i w_{li}(y_{li}^o - y_{li}^c)^2/\upsilon \qquad (8)$$

where the index l sums over q experiments, and the index i sums over the appropriate channel limits for each individual experiment. y_{li}^o and y_{li}^c denote respectively the observed and calculated (fitted) values corresponding to the ith channel of the lth experiment, and w_{li} is the corresponding statistical weight. υ represents the number of degrees of freedom for the entire multidimensional fluorescence decay surface.

The statistical criteria to judge the quality of the fit included both graphical and numerical tests and have been described previously.[39] The decays were analyzed first individually by a (multi)exponential decay law in terms of decay times τ_i and their associated pre-exponential factors α_i. The final curve-fitting was done by global (or simultaneous) analysis in which decay traces recorded at several emission wavelengths were described by a (multi)exponential decay function with linked (global) decay times τ_i and local pre-exponentials α_i. A minimum of four different observation wavelengths covering the emission spectrum were selected for the construction of the fluorescence decay surface. The quality of the fit was judged for each fluorescence decay trace separately as well as for the global fluorescence decay surface. All reported curve fittings had χ^2 values below 1.1.

4.6. Determination of K_d via Direct Fluorometric Titration. The ground-state dissociation constants K_d of the complexes between **1** and various cations were determined in CH_3CN solution at 20 °C by *direct* fluorometric titration as a function of the cation concentration [X] using the fluorescence−excitation or emission spectra (at least four independent measurements were used to compute the average K_d value). Nonlinear fitting of eq 6[40] to the steady-state fluorescence data F recorded as a function of [X] yields values of K_d, F_{min}, F_{max}, and n. Because the fits of eq 6 to the fluorescence data F with n, K_d, F_{min}, and F_{max} as freely adjustable parameters always gave values of n close to 1, n was kept fixed at 1 in the final curve fittings, from which the estimated K_d values are reported here.

4.7. Determination of K_d via Ratiometric Fluorometric Titration. Fitting eq 7 to *excitation* ratiometric values $R = F(\lambda_{em},\lambda_{ex}^1)/F(\lambda_{em},\lambda_{ex}^2)$ as a function of the cation concentration [X] yields values for $K_d\xi(\lambda_{em},\lambda_{ex}^2)$, n, R_{min}, and R_{max}. Because $\xi(\lambda_{em},\lambda_{ex}^2)$, the ratio of the fluorescence signal of the free form of the indicator over that of the bound form at the indicated wavelengths, is experimentally accessible, a value for K_d can be recovered from ratiometric excitation fluorescence data.

In a similar way, fitting eq 7 to the *emission* ratiometric fluorescence data $R = F(\lambda_{em}^1,\lambda_{ex})/F(\lambda_{em}^2,\lambda_{ex})$ as a function of the cation concentration [X] yields values for $K_d\xi(\lambda_{em}^2,\lambda_{ex})$, n, R_{min}, and R_{max}. Because $\xi(\lambda_{em}^2,\lambda_{ex})$ can be determined from the fluorescence signals of the free and bound forms of the indicator at the indicated wavelengths, a value K_d for can be obtained.

5. Theoretical Methodology

The ground-state potential energy surface of the pristine molecule and the alkali complex was first explored at the force field level (on the basis of the Universal Force Field (UFF)[41]). Two successive molecular dynamics (MD) simulations were performed at 600 K for 1 ns each. The geometry of the most stable conformers extracted from these MD runs was then optimized at 0 K. The UFF geometries were then refined at the DFT level using the B3LYP functional and the 6-311g** basis set. The same approach was applied for the protonated structure.

The DFT geometries were used as entries for excited-state calculations performed at the INDO/SCI level.[42] The active space included the 50th nearest orbitals of the system.

Acknowledgment. We thank the University Research Fund of the K.U.Leuven for Grant GOA 2001/2, 2006/2, and IDO/00/001, and for postdoctoral fellowships to M.B. and W.Q. The IAP-V-03 and VI-27 programs are thanked for a fellowship to M.S. The Fonds voor Wetenschappelijk Onderzoek-Vlaanderen (FWO) is acknowledged for grant G.0320.00N. The Instituut voor de aanmoediging van innovatie door Wetenschap en Technologie in Vlaanderen (IWT) is acknowledged for grant ZWAP 04/007. D.B. is a research associate of the Belgian Fonds National de la Recherche Scientifique (FNRS). B.V.A. thanks the Fonds pour la Recherche en Industrie et en Agriculture (FRIA) for financial support.

Supporting Information Available: Absorption, fluorescence−excitation and emission spectra of **1** in acetonitrile in as a function of [Li^+], [Na^+], [Mg^{2+}], [Ca^{2+}], and [Zn^{2+}]. ^1H NMR spectrum of **1** in $CDCl_3$. This material is available free of charge via the Internet at http://pubs.acs.org.

References and Notes

(1) Desvergne, J.-P., Czarnik, A. W. Eds. *Chemosensors of Ion and Molecule Recognition*; Kluwer: Dordrecht, The Netherlands, 1997.

(2) Haugland, R. P. *The Handbook. A Guide to Fluorescent Probes and Labeling Technologies*, 10th ed.; Molecular Probes, Inc.: Eugene, OR, 2005.

(3) Valeur, B., Brochon, J.-C. Eds. *New Trends in Fluorescence Spectroscopy. Applications to Chemical and Life Sciences*; Springer: Berlin, 2002.

(4) Treibs, A.; Kreuzer, F.-H. *Liebigs Ann. Chem.* **1968**, *718*, 208–223.

(5) Ziessel, R.; Ulrich, G.; Harriman, A. *New J. Chem.* **2007**, *31*, 496–501.

(6) Loudet, A.; Burgess, K. *Chem. Rev.* **2007**, *107*, 4891–4932.

(7) (a) Baruah, M.; Qin, W.; Basarić, N.; De Borggraeve, W. M.; Boens, N. *J. Org. Chem.* **2005**, *70*, 4152–4157. (b) Qin, W.; Baruah, M.; Stefan, A.; Van der Auweraer, M.; Boens, N. *ChemPhysChem.* **2005**, *6*, 2343–2351.

(8) Qin, W.; Baruah, M.; De Borggraeve, W. M.; Boens, N. *J. Photochem. Photobiol. A: Chem.* **2006**, *183*, 190–197.

(9) Yamada, K.; Nomura, Y.; Citterio, D.; Iwasawa, N.; Suzuki, K. *J. Am. Chem. Soc.* **2005**, *127*, 6956–6957.

(10) Malval, J.-P.; Leray, I.; Valeur, B. *New. J. Chem.* **2005**, *29*, 1089–1094.

(11) Baruah, M.; Qin, W.; Vallée, R. A. L.; Beljonne, D.; Rohand, T.; Dehaen, W.; Boens, N. *Org. Lett.* **2005**, *7*, 4377–4380.

(12) Basarić, N.; Baruah, M.; Qin, W.; Metten, B.; Smet, M.; Dehaen, W.; Boens, N. *Org. Biomol. Chem.* **2005**, *3*, 2755–2761.

(13) Coskun, A.; Akkaya, E. U. *J. Am. Chem. Soc.* **2005**, *127*, 10464–10465.

(14) Wu, Y.; Peng, X.; Guo, B.; Fan, J.; Zhang, Z.; Wang, J.; Cui, A.; Gao, Y. *Org. Biomol. Chem.* **2005**, *3*, 1387–1392.

(15) Seo, T. S.; Bai, X.; Kim, D. H.; Meng, Q.; Shi, S.; Ruparel, H.; Li, Z.; Turro, N. J.; Ju, J. *Proc. Natl. Acad. Sci. USA* **2005**, *102*, 5926–5931.

(16) Yee, M.-c.; Fas, S. C.; Stohlmeyer, M. M.; Wandless, T. J.; Cimprich, K. A. *J. Biol. Chem.* **2005**, *280*, 29053–29059.

(17) (a) Vos de Wael, E.; Pardoen, J. A.; van Koeveringe, J. A.; Lugtenburg, J. *Recl. Trav. Chim. Pays-Bas* **1977**, *96*, 306–309. (b) Karolin, J.; Johansson, L. B.-Å.; Strandberg, L.; Ny, T. *J. Am. Chem. Soc.* **1994**, *116*, 7801–7806. (c) López Arbeloa, T.; López Arbeloa, F.; López Arbeloa, I.; García-Moreno, I.; Costela, A.; Sastre, R.; Amat-Guerri, F. *Chem. Phys. Lett.* **1999**, *299*, 315–321. (d) Rurack, K.; Kollmannsberger, M.; Daub, J. *Angew. Chem., Int. Ed.* **2001**, *40*, 385–387. (e) Bergström, F.; Mikhalyov, I.; Hägglöf, P.; Wortmann, R.; Ny, T.; Johansson, L. B.-Å. *J. Am. Chem. Soc.* **2002**, *124*, 196–204. (f) Costela, A.; García-Moreno, I.; Gomez, C.; Sastre, R.; Amat-Guerri, F.; Liras, M.; López Arbeloa, F.; Bañuelos Prieto, J.; López Arbeloa, I. *J. Phys. Chem. A.* **2002**, *106*, 7736–7742. (g) López Arbeloa, F.; Bañuelos Prieto, J.; Martínez Martínez, V.; Arbeloa López, T.; López Arbeloa, I. *ChemPhysChem* **2004**, *5*, 1762–1771. (h) Bañuelos Prieto, J.; Lüpez Arbeloa, F.; Martínez Martínez, V.; Arbeloa López, T.; Amat-Guerri, F.; Liras, M.; López Arbeloa, I. *Chem. Phys. Lett.* **2004**, *385*, 29–35. (i) Qin, W.; Rohand, T.; Baruah, M.; Stefan, A.; Van der Auweraer, M.; Dehaen, W.; Boens, N. *Chem. Phys. Lett.* **2006**, *420*, 562–568.

(18) Kollmannsberger, M.; Rurack, K.; Resch-Genger, U.; Daub, J. *J. Phys. Chem. A* **1998**, *102*, 10211–10220.

(19) Qin, W.; Baruah, M.; Van der Auweraer, M.; De Schryver, F. C.; Boens, N. *J. Phys. Chem. A* **2005**, *109*, 7371–7384.

(20) Bourson, J.; Valeur, B. *J. Phys. Chem.* **1989**, *93*, 3871–3876.

(21) Létard, J.-F.; Lapouyade, R.; Rettig, W. *Pure Appl. Chem.* **1993**, *65*, 1705–1712.

(22) Rurack, K.; Kollmannsberger, M.; Resch-Genger, U.; Daub, J. *J. Am. Chem. Soc.* **2000**, *122*, 968–969.

(23) Bricks, J. L.; Kovalchuk, A.; Trieflinger, C.; Nofz, M.; Büschel, M.; Tolmachev, A. I.; Daub, J.; Rurack, K. *J. Am. Chem. Soc.* **2005**, *127*, 13522–13529.

(24) Baruah, M.; Qin, W.; Flors, C.; Hofkens, J.; Vallée, R. A. L.; Beljonne, D.; Van der Auweraer, M.; De Borggraeve, W. M.; Boens, N. *J. Phys. Chem. A* **2006**, *110*, 5998–6009.

(25) van der Meer, M. J.; Zhang, H.; Rettig, W.; Glasbeek, M. *Chem. Phys. Lett.* **2000**, *320*, 673–680.

(26) Lippert, E. *Z. Naturforsch., A: Phys. Sci.* **1955**, *10*, 541–545.

(27) Mataga, N.; Kaifu, Y.; Koizumi, M. *Bull. Chem. Soc. Jpn.* **1955**, *28*, 690–691, and **1956**, *29*, 465−470.

(28) Reichardt, C. *Chem. Rev.* **1994**, *94*, 2319–2358.

(29) Kamlet, M. J.; Taft, R. W. *J. Am. Chem. Soc.* **1976**, *98*, 377–383.

(30) Catalán, J. *J. Org. Chem.* **1997**, *62*, 8231–8234.

(31) *Handbook of Solvents*; Wypych, G., Ed.; ChemTec Publishing: Toronto, 2001; pp 583−616.

(32) Catalán, J.; Palomar, J.; Díaz, C.; de Paz, J. L. G. *J. Phys. Chem. A* **1997**, *101*, 5183–1589.

(33) Marcus, Y. *Chem. Soc. Rev.* **1993**, *22*, 409–416.

(34) Catalán, J.; Hopf, H. *Eur. J. Org. Chem.* **2004**, 4694–4702.

(35) Birks, J. B. *Photophysics of Aromatic Molecules*; Wiley-Interscience: London, 1970.

(36) Olmsted, J. *J. Phys. Chem.* **1979**, *83*, 2581–2584.

(37) (a) O'Connor, D. V.; Phillips, D. *Time-correlated Single Photon Counting*; Academic Press: New York, 1984. (b) vandeVen, M.; Ameloot, M.; Valeur, B.; Boens, N. *J. Fluorescence* **2005**, *15*, 377–413. (c) Boens, N.; Qin, W.; Basarić, N.; Hofkens, J.; Ameloot, M.; Pouget, J.; Lefèvre, J.-P.; Valeur, B.; Gratton, E.; vandeVen, M.; Silva, N. D.; Engelborghs, Y.; Willaert, K.; Sillen, A.; Rumbles, G.; Phillips, D.; Visser, A. J. W. G.; Van Hoek, A.; Lakowicz, J. R.; Malak, H.; Gryczynski, I.; Szabo, A. G.; Krajcarski, D. T.; Tamai, N.; Miura, A. *Anal. Chem.* **2007**, *79*, 2137–2149.

(38) Crovetto, L.; Orte, A.; Talavera, E. M.; Alvarez-Pez, J. M.; Cotlet, M.; Thielemans, J.; De Schryver, F. C.; Boens, N. *J. Phys. Chem. B* **2004**, *108*, 6082–6092.

(39) Van den Zegel, M.; Boens, N.; Daems, D.; De Schryver, F. C. *Chem. Phys.* **1986**, *101*, 311–335.

(40) Cielen, E.; Tahri, A.; Ver Heyen, A.; Hoornaert, G. J.; De Schryver, F. C.; Boens, N. *J. Chem. Soc., Perkin Trans. 2* **1998**, 1573–1580.

(41) Rappé, A. K.; Casewit, C. J.; Colwell, K. S.; Goddard, W. A.; Skiff, W. M. *J. Am. Chem. Soc.* **1992**, *114*, 10024–10035.

(42) Zerner, M. C.; Loew, G. H.; Kirchner, R. F.; Mueller-Westerhoff, U. T. *J. Am. Chem. Soc.* **1980**, *102*, 589–599.

JP800261V